Research Article | Vol. 27, No. 26 / 23 December 2019 / Optics Express 37122
Optics EXPRESS

Ultrahigh temperature and strain hybrid integrated sensor system based on Raman and femtosecond FBG inscription in a multimode gold-coated fiber

I. LAAROSSI,[1,*] P. ROLDÁN-VARONA,[1] M. A. QUINTELA-INCERA,[1,2,3] L. RODRÍGUEZ-COBO,[2] AND J. M. LÓPEZ-HIGUERA[1,2,3]

[1] *Photonics Engineering Group, University of Cantabria, 39005, Santander, Spain*
[2] *CIBER-bbn, Instituto de Salud Carlos III, 28029, Madrid, Spain*
[3] *Instituto de Investigación Sanitaria Valdecilla (IDIVAL), 39011, Santander, Spain*
[*] *laarossii@unican.es*

Abstract: In this paper, a novel approach for hybrid systems combining Raman distributed sensors with fiber Bragg grating (FBG) sensors to carry out distributed and quasi-distributed temperature/strain measurements was proposed and experimentally demonstrated. Three FBGs were inscribed by the point-by-point technique in a simple setup for type I femtosecond inscription in a pure silica core multimode gold-coated fiber. Employing a single fiber, temperatures up to 600 $°C$ and strains up to 4144 $\mu\varepsilon$ approximately were measured simultaneously and without interferences between both distributed and point measurements. Moreover, a new calibration technique was implemented to calibrate the distributed temperature system using the FBG measurements as reference.

1. Introduction

Over recent years, optical fiber sensors have gained increasing attention in both scientific and industrial fields.[1]. Some of their unique properties, such as electromagnetic immunity, chemical resistance, their ability to work in hostile environments, flexibility and multiplexing capabilities make them an attractive solution against conventional sensors [2].

Among the different types of optical fiber sensors, fiber Bragg grating (FBG) and Raman-based distributed temperature sensors (RDTS) are to-date the most widely used and desired by many fields of industry for both quasi-distributed and distributed measurements [3,4]. Furthermore, the combination of these two technologies is of great interest in industrial environments because it allows a complete sensing of different structures: distributed temperature measurements along the structure and also strain/temperature measurements in areas of special interest, where the distributed sensing does not have the required spatial resolution. Moreover, it offers a low-cost and low-complexity systems in comparison to other alternatives presented in the associated literature [5,6].

In general, Raman distributed temperature sensors are based on multimode fibers for ranges up to 40 km [7] since these fibers have higher backscatter coefficients and stimulated Raman scattering threshold power (SRS), which improves the signal-to-noise (SNR) ratio in the backscattered Raman signals [8]. However, the state of the art in multimode FBGs is not as extensive as in single mode fibers (SMF). Some previous works [9–11] have calculated the theoretical spectrum of multimode FBGs, experimentally characterizing their response and proposing applications such as bending sensors or longitudinal strain measurement. In addition, most multimode FBGs are based on the UV FBG inscription, which directly implies a poor temperature resistance, thus being

#372478 https://doi.org/10.1364/OE.27.037122
Journal © 2019 Received 18 Jul 2019; revised 28 Sep 2019; accepted 19 Oct 2019; published 9 Dec 2019
Corrected: 23 Dec 2019

Optics EXPRESS

completely erased at temperatures around 600 °C [12]. This fact leaves unattended the growing demand to develop sensors that operate permanently in these temperature ranges. Therefore, it is necessary to use the FBG inscription via femtosecond laser to increase its operating ranges to more than 800 °C [13]. In addition, this method simplifies the manufacturing complexity of these sensors, avoiding the hydrogen loading treatment.

In this work, a new and highly efficient hybrid system is presented and experimentally demonstrated for the simultaneous measurement of high temperature and strain, combining two of the most commonly used and low-cost technologies in optical fiber sensing. Distributed and quasi-distributed temperature measurements were carried out up to 600 °C using a Raman Optical-Time-Domain-Reflectometry (ROTDR) system with pure silica multimode gold-coated fiber and FBGs inscribed in the same multimode fiber. The FBGs were fabricated employing the point-by-point (PbP) technique in a simple setup for Type I femtosecond inscription and their notable resistance to high temperatures and strain up to 4144 $\mu\varepsilon$ approximately were demonstrated. Finally, profiting the hybrid system proposed, a new calibration approach was implemented in the ROTDR measurements to correct the dynamic variations with temperature of optical losses in the gold-coated fiber.

2. FBG manufacturing

The FBG inscriptions were performed using a commercial femtosecond laser FLCPA (CALMAR lasers), operating at 1030 nm, with a 370 fs pulse duration, a maximum pulse repetition rate (PRR) of 120 kHz and a spot diameter of 0.8 ± 0.2 μm. Laser pulses were focused through an $x100/NA = 0.5$ objective lens from Mitutoyo, converging on the fiber, which is located between a slide and a coverslip. Between them an index-matching oil with refractive index similar to the fiber cladding (1.4646, approximately) has been deposited to eliminate the spherical aberration of the fiber itself, thus increasing the fluence in the focal volume. The slide, where the fiber is located, is placed in a platform fixed to a nanoresolution XYZ motor from Aerotech.

The FBGs, each one with a length of $L_{FBG} = 5\ mm$, were inscribed into a 50/125 μm graded-index multimode pure silica gold-coated fiber by means of the point-by-point (PbP) method using a single shot per point with a pulse energy of 0.47 μJ and a PRR of 20 Hz. The chosen pulse energy causes a smooth and isotropic refractive index change (RIC), classified as Type I within the RIC induced by the femtosecond laser. This RIC was estimated by the refracted near field profilometry technique, obtaining a value of $\Delta n = |n_{spot} - n_{core}| \approx 3 \cdot 10^{-3}$, where n_{spot} and n_{core} are the refractive index of the change generated by each pulse and the core fiber refractive

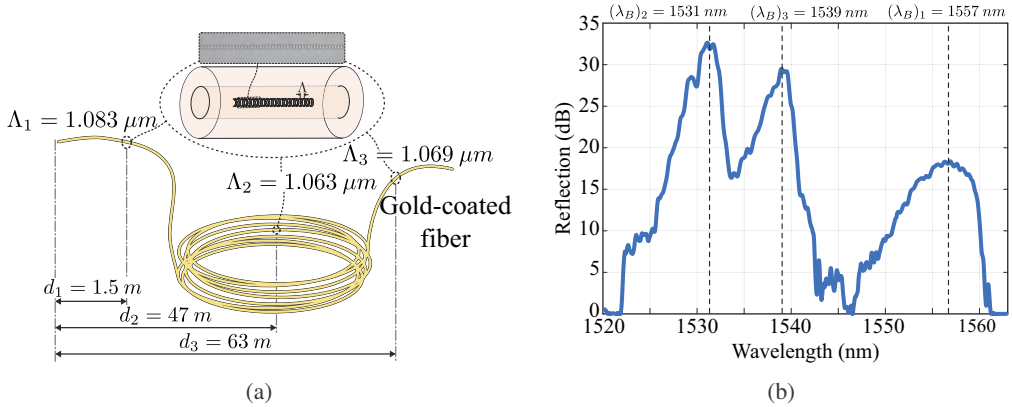

(a) (b)

Fig. 1. (a) Schematic diagram of FBGs (with their corresponding period, Λ) location in the gold-coated fiber, (b) Reflection spectra at room temperature and without strain.

Optics EXPRESS

index, respectively. In order to discern the FBGs, each one was manufactured with a different period: $\Lambda_1 = 1.083\ \mu m$, $\Lambda_2 = 1.063\ \mu m$ and $\Lambda_3 = 1.069\ \mu m$ that correspond with $\lambda_1 = 1557\ nm$, $\lambda_2 = 1531\ nm$ and $\lambda_3 = 1539\ nm$, respectively. All of them lie in the C-band, using for it the second Bragg wavelength.

The three FBGs were inscribed at distances of 1.5 m, 47 m and 63 m from the start end of the gold-coated fiber. The period of each one determines the scan speed for its inscription through the relationship: $v = \Lambda \cdot PRR$. Therefore, the maximum inscription time takes place when the FGB with Λ_2 is inscribed: $t_{max} = L_{FBG}/v_{min} = 5\ mm/(1.063\ \mu m \cdot 20\ Hz) \approx 4\ min$. Figure 1 (a) describes the spatial arrangement of the FBGs along the fiber and Fig. 1 (b) shows the spectrum measured at room temperature and without strain.

3. Experimental setup and results

3.1. Experimental setup

The setup designed and employed in the experimental tests is schematically shown in Fig. 2. The fiber under test (FUT) is formed by two spools of standard silica graded-index multimode fiber (with lengths of 264 m and 16.5 m) spliced to the both ends of a 67 m of a pure silica gold-coated fiber.

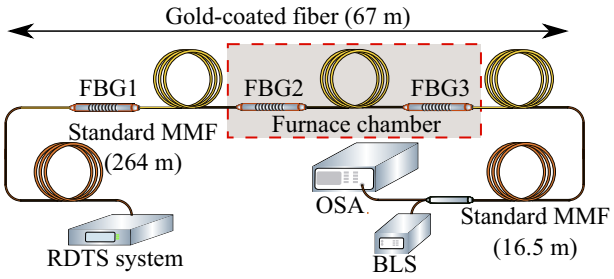

Fig. 2. Schematic diagram of the hybrid Raman/FBGs experimental setup.

At one end of the FUT (at the free end of the multimode fiber with length of 264 m), a Raman distributed temperature sensor (RDTS) system based on Optical-Time-Domain-Reflectometry (OTDR) was employed to carry out the temperature distributed measurements. The light source of the sensor unit is given by a laser centered at 1064 nm, providing 5 ns duration pulses and an average output power of 17 mW. Therefore, the three type I femtosecond inscribed FBGs in the multimode gold-coated fiber are arranged at 265.5 m, 311 m, and 327 m from the RDTS system, respectively.

In order to measure the reflecting FBGs, the port 2 of a broadband optical circulator (1460 – 1620 nm) was spliced at the other end of the FUT. The FBGs were illuminated with a broadband light source (BLS) (HP 83437A) connected to port 1 of the circulator and the spectra of the FBGs were measured with an optical spectrum analyzer (OSA) (Anritsu MS9740A) connected to port 3. The BLS incorporate four broadband LEDs, providing a large spectrum in the 1200 nm to 1700 nm range. The spectra measurements have been carried out with a resolution of 0.1 nm

18 m of gold-coated fiber (including two FBGs: FBG2 and FBG3) were placed within a high temperature furnace chamber and a thermal cycle between room temperature (22°C approximately) and 600 °C with steps of 50 °C was programmed to demonstrate and validate the proposed approach.

Moreover, concerning the strain characterization of FBGs 1 and 2, measurements were performed stretching the fiber by means of two XYZ platforms (one fixed and the other one

Optics EXPRESS

movable). Initially, the two platforms are separated a distance $d = 15.2\ cm$ and the FBGs are placed completely stretched. After that, the distance was gradually increased (moving the movable platform on the X axis) by steps of 0.03 *mm* (equivalent to 200 $\mu\varepsilon$) up to 0.63 *mm*, increasing the applied strain. The maximum applied strain was 4144 $\mu\varepsilon$, approximately. Figure 3 shows the diagram of the employed setup.

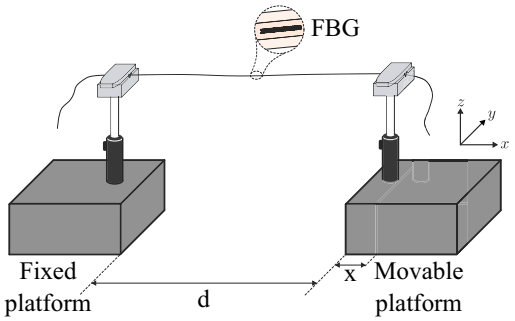

Fig. 3. Schematic diagram of the setup employed for strain characterization.

3.2. Experimental results

Distributed temperature measurements were performed after leaving enough time until the temperature was stable inside the furnace, at each programmed temperature. The measurement time and the spatial resolution of each trace were 60 *s* and 0.5 *m*, respectively. The anti-Stokes (AS) and Stokes (S) signal traces (at $\lambda_{AS} = 1014\ nm$ and $\lambda_S = 1114\ nm$) for the entire FUT are shown in Fig. 4.

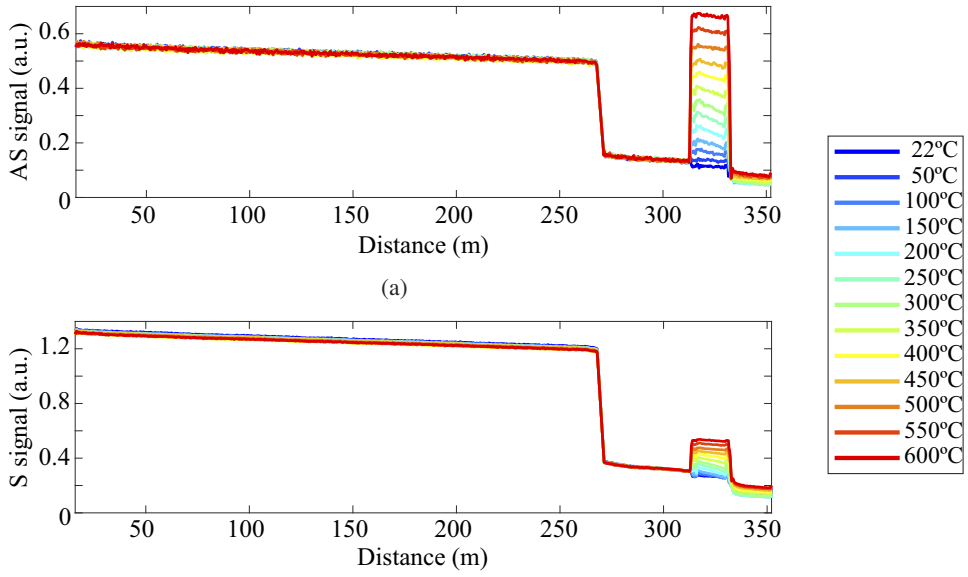

Fig. 4. (a) Anti-Stokes and (b) Stokes signals for the entire FUT.

It can be observed that the anti-Stokes and Stokes signals traces obtained from the gold-coated fiber are noisier than the traces recovered from the standard MMF. This, is due to the macrobends exhibited by this type of fibers. Moreover, the high power generated in the standard MMF

Optics EXPRESS

compared to the pure silica gold-coated fiber [14] and the splice point between both fibers, generate an abrupt decay in the power of the AS and S signals, can be appreciated in the 264 m distance. In addition, it can also be noted that there are no reflections in the backscattered Raman signals at the positions of the three inline FBGs. This is mainly due to the large separation between the operating wavelengths of the Raman unit and those used by the configuration employed to interrogate the FBGs.

Although the intensity of the anti-Stokes signal is strongly dependent on temperature, in RDTS systems, it is common to use the ratio between the power of the both Raman components ($P_{AS}(z,T)$ and $P_S(z,T)$) to determine the temperature profile along the fiber. On these basis, the problems related with the dependence of the AS signal on other parameters, such as the attenuation at AS wavelength, local losses in the fiber, splices, etc. can be overcome. The analytical expression of this ratio can be expressed by [15]:

$$R(z) = \frac{P_{AS}(z,T(z))}{P_S(z,T(z))} = C_R e^{-\frac{h\Delta\nu}{kT(z)}} e^{-\int_0^z \Delta\alpha(z')dz'} \tag{1}$$

where $T(z)$ is the absolute temperature, z is the distance along the fiber and C_R is a constant which depends on different parameters, such as, Raman capture factor and the response of the receiver. $\Delta\nu$, h and k are the frequency separation between AS and pump signal, Planck and Boltzmann constants, respectively; $\Delta\alpha = \alpha_{AS} - \alpha_S$ is the differential attenuation, being α_{AS} and α_S the fiber attenuation coefficients at λ_{AS} and λ_S, respectively. From Eq. 1, the distributed temperature profile $T(z)$ can be calculated as:

$$T(z) = -\frac{h\Delta\nu}{k\left[\ln\left[R(z)\right] - \ln\left[C_R\right] + \int_0^z \Delta\alpha(z')dz'\right]} \tag{2}$$

C_R and $\Delta\alpha$ values were calculated in the calibration process before beginning the measurements, keeping a fiber section in a constant and uniform temperature. Under consideration of optical fiber maintains its attenuation spectrum over time, the differential attenuation keeps constant with time and its value was calculated as the slope of the line that adjusts $\ln(R(z))$ with z in this section [16]. $h\Delta\nu/k$ was fixed to its theoretical value, $h\Delta\nu/k = 490$ [17].

The temperature profiles, calculated from Eq. 2, along the entire FUT and obtained at the different programmed temperatures are depicted in Fig. 5. It is worth noting that the small variations observed in the hot-spot section for each temperature are a consequence of the macrobends mentioned above. Furthermore, the non-uniform profile of the losses presented by gold-coated fibers and its variations with temperature induce high errors in the calculated temperature [18,19]. The error committed in the temperature estimation, calculated as the difference between the average value of the hot-spot section and the programmed temperature, is also shown in Fig. 5. As can be noticed, the errors increase as temperature rises, reaching a maximum of 49 $^\circ C$, approximately, at 600 $^\circ C$.

On the other hand, the spectra of the FBGs 2 and 3 was captured throughout the programmed thermal cycle, simultaneously with the distributed measurements. The time between two consecutive measurements and the total measurement time were 150 s and 354 minutes, respectively. A 3D representation of the obtained results is presented in Fig. 6 (a). As can be seen, the reflection spectra of FBG 2 and 3 are displaced with temperature. In addition, the reflection peak power of these FBGs remains practically constant when temperature increases, unlike what happens with the FBG based on UV inscription [12,20]. In order to compare the results obtained by these FBGs and the hot-spot section of the FUT, Fig. 6 (b) shows the shift of the maximum reflection wavelength of the captured spectra at stable temperatures. As a result, the temperature sensitivity of both FBGs was calculated throughout the measurement range (from room temperature to 600 $^\circ C$), resulting in 12.39 $pm/^\circ C$ and 13.06 $pm/^\circ C$ for FBG 2 and 3, respectively.

Optics EXPRESS

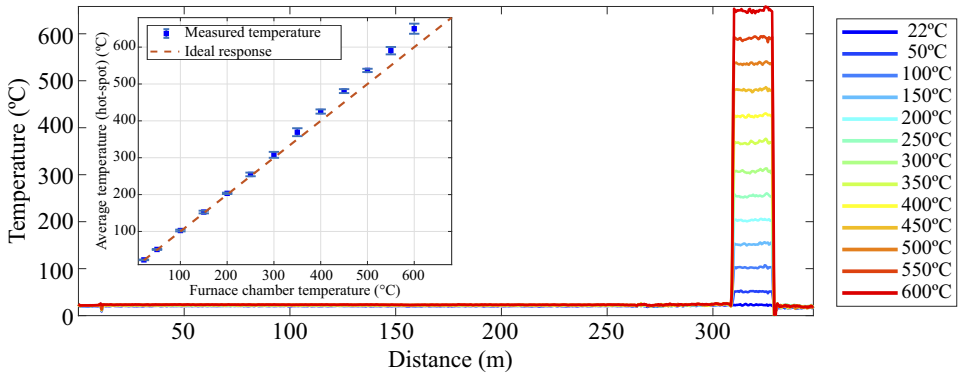

Fig. 5. Measurement temperature profile for the entire FUT.

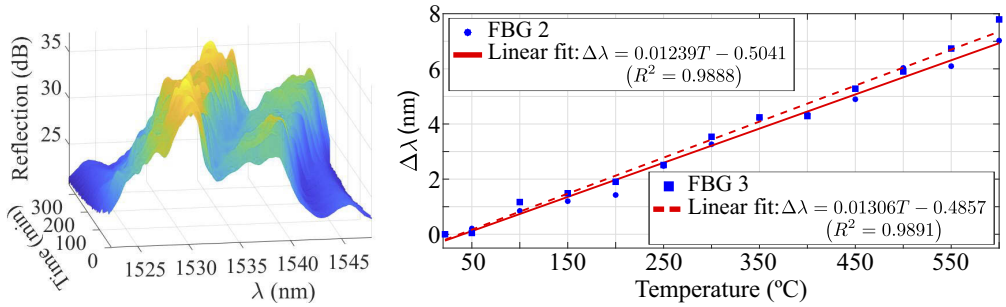

(a) (b)

Fig. 6. (a) 3D representation of the spectra captured throughout the programmed thermal cycle, (b) the Bragg wavelength shift as a function of temperature.

The strain measurements accomplished with FBG 1 using the configuration described in Fig. 3 in the FBG 1 are depicted in the Fig. 7 (a). Regarding the obtained results, it can be observed that the variation of the reflected spectra as a function of the strain applied shows a high linearity.

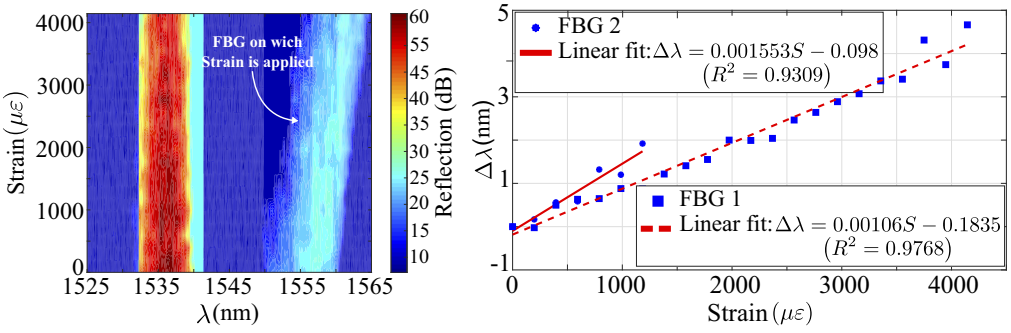

(a) (b)

Fig. 7. (a) Reflectivity spectra of the FBG 1,(b) the Bragg wavelength shift as a function of strain.

To estimate the sensitivity of both FBGs, a linear fit for wavelength shift as a function of strain was calculated, Fig. 7 (b) reports the results obtained. Since the FBG 2 was subjected to high

Optics EXPRESS

temperatures (up to 600 $^{\circ}C$) and trying to prevent its break, the maximum applied strain was 1184 $\mu\varepsilon$, approximately. The two FBGs exhibit a very good linear response, having a sensitivity around 1.55 $pm/\mu\varepsilon$ and 1.06 $pm/\mu\varepsilon$, approximately.

In both cases, the obtained temperature and strain are very similar to those reported in the literature for FBGs inscribed in SMF. For example, the strain sensitivity measured in [21] and [22] was 1.10 $pm/\mu\varepsilon$ and 1.5 $pm/\mu\varepsilon$, respectively. Whereas in [23] the temperature sensitivity reported was 13.7 $pm/^{\circ}$C.

An important advantage of this hybrid system is that the FBGs will allow to correct the errors of temperature distributed measurements in the multimode gold-coated fiber at the different programmed temperatures. The temperature measured with FBGs 2 and 3 will be used as a reference to carry out the calibration process of the distributed sensor system. In this way, and as long as the two FBGs are at the same temperature as the section subjected to temperature variations and the FBG 1 is at same strain as the other two FBGs (for the purpose of carrying out the strain-temperature discrimination in FBGs 2 and 3), it is possible to minimize the errors committed in the temperature estimation. For this aim, the cross-sensitivity of the two parameters (strain and temperature) was studied to discriminate strain contribution to the FBGs wavelength shifts in the hot-spot section. Knowing the variations of both variables and using the sensitivity coefficients previously calculated, the Bragg wavelength shifts are given by [24]:

$$\begin{bmatrix} \Delta\lambda_1 \\ \Delta\lambda_2 \end{bmatrix} = \begin{bmatrix} KT_1 & K\varepsilon_1 \\ KT_2 & K\varepsilon_2 \end{bmatrix} \begin{bmatrix} \Delta T \\ \Delta\varepsilon \end{bmatrix} \tag{3}$$

where $\Delta\lambda_1$ and $\Delta\lambda_2$ are the wavelength shifts of the FBG 1 and 2, respectively. KT is the temperature sensitivity and $K\varepsilon$ is the strain sensitivity coefficient; ΔT and $\Delta\varepsilon$ are the temperature and strain variations, respectively. Rewriting Eq. 3, it is possible to determine the two variables variations:

$$\begin{bmatrix} \Delta T \\ \Delta\varepsilon \end{bmatrix} = \frac{1}{D} \begin{bmatrix} K\varepsilon_2 & -K\varepsilon_1 \\ -KT_2 & KT_1 \end{bmatrix} \begin{bmatrix} \Delta\lambda_1 \\ \Delta\lambda_2 \end{bmatrix} \tag{4}$$

being D the matrix determinant. Figure 8 depicts the cross-sensitivity of temperature and strain, which was obtained by fixing one measurand and varying the other one, in both cases. The applied sweeps (temperature and strain) are depicted (black dotted lines) against the values estimated by Eq. 4 (dots).

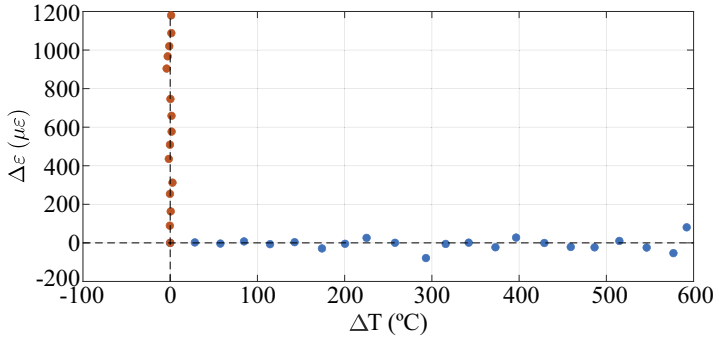

Fig. 8. Cross-sensitivity of temperature and strain.

Once the strain contribution has been discriminated in the FGBs located inside the furnace chamber, distributed measurements were calibrated using the FBGs temperatures as reference. Figure 9 (a) shows the results obtained from applying this approach to the hot-spot section of the

Optics EXPRESS

temperature profiles presented above in the Fig. 5. As can be observed in Fig. 9 (b), the errors were significantly reduced, minimizing the maximum error (at 600 $^{\circ}C$) up to 6 $^{\circ}C$,approximately.

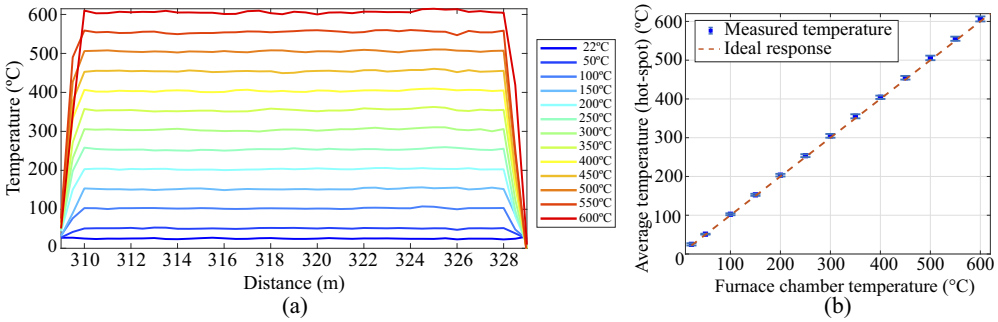

Fig. 9. (a) Hot-spot section temperature profile after applying the corrections, (b) Temperature error.

4. Conclusion

In this work, a hybrid system based on Raman DTS and femtosecond laser FBGs sensors was developed and its high performance was demonstrated. Distributed and quasi-distributed temperature/strain measurements were carried out fusing the two most used kinds of optical fiber sensors in a single metal-coated fiber. Measurements up to 600 $^{\circ}C$ and strains up to 4144 $\mu\varepsilon$ were experimentally measured simultaneously and without interferences. The type I FBGs inscribed in the gold-coated fiber exhibit a linear behavior throughout the whole measurement range both in temperature and strain, maintaining its initial characteristics. Finally, the distributed temperature measurements were corrected, eliminating errors due to the variation of the optical losses, using the FBG measurements as reference.

Funding

Spanish Government FEDER Funds (TEC2016-76021-C2-2-R).

References

1. A. Ukil, H. Braendle, and P. Krippner, "Distributed temperature sensing: Review of technology and applications," IEEE Sens. J. **12**(5), 885–892 (2012).
2. J. M. López-Higuera, *Handbook of Optical Fibre Sensing Technology* (Willey, 2014).
3. J. P. Dakin, K. Hotate, R. A. Lieberman, and M. A. Marcus, "Optical fiber sensors," in *Handbook of Optoelectronics*, (CRC, 2017).
4. Y. Bao, Y. Huang, M. S. Hoehler, and G. Chen, "Review of fiber optic sensors for structural fire engineering," Sensors **19**(4), 877–900 (2019).
5. A. Zornoza, R. A. Pérez-Herrera, C. Elosúa, S. Diaz, C. Bariain, A. Loayssa, and M. Lopez-Amo, "Long-range hybrid network with point and distributed Brillouin sensors using Raman amplification," Opt. Express **18**(9), 9531–9541 (2010).
6. F. Li, W. Zhao, H. Xu, S. Wang, and Y. Du, "A highly integrated BOTDA/XFG sensor on a single fiber for simultaneous multi-parameter monitoring of slopes," Sensors **19**(9), 2132–2148 (2019).
7. A. Signorini, S. Faralli, M. A. Soto, G. Sacchi, F. Baronti, R. Barsacchi, A. Lazzeri, R. Roncella, G. Bolognini, and F. Di Pasquale, "40 km long-range Raman-based distributed temperature sensor with meter-scale spatial resolution," In *Opt. Fiber Commun. Conf. Opt. Soc. Am.*, OWL2 (2010).
8. M. Wang, H. Wu, M. Tang, Z. Zhao, Y. Dang, C. Zhao, R. Liao, W. Chen, S. Fu, C. Yang, W. Tong, P. P. Shum, and W. Tong, "Few-mode fiber based Raman distributed temperature sensing," Opt. Express **25**(5), 4907–4916 (2017).
9. M. J. Schmid and M. S. Muller, "Measuring Bragg gratings in multimode optical fibers," Opt. Express **23**(6), 8087–80948 (2015).
10. X. Sang, C. Yu, and B. Yan, "Bragg gratings in multimode optical fibres and their applications," J. Optoelectron. Adv. Mater. **8**, 1616–1622 (2006).

Optics EXPRESS

11. R. M. Cazo, O. Lisboa, H. T. Hattori, V. M. Schneider, C. L. Barbosa, R. C. Rabelo, and J. L. S. Ferreira, "Experimental analysis of reflected modes in a multimode strained grating," Microw. Opt. Technol. Lett. **28**(1), 4–8 (2001).
12. S. J Mihailov, D. Grobnic, C. Hnatovsky, R. B Walker, P. Lu, D. Coulas, and H. Ding, "Extreme Environment Sensing Using Femtosecond Laser-Inscribed Fiber Bragg Gratings," Sensors **17**(12), 2909–2942 (2017).
13. B. Pal, *Frontiers in guided wave optics and optoelectronics* (IntechOpen, 2010).
14. M. A. Farahani and T. Gogolla, "Spontaneous Raman scattering in optical fibers with modulated probe light for distributed temperature Raman remote sensing," J. Lightwave Technol. **17**(8), 1379–1391 (1999).
15. M. A. Soto and F. Di Pasquale, "Distributed Raman Sensing," in *Handbook of Optical Fibers* (Springer, 2018).
16. M. B. Hausner, F. Suárez, K. E. Glander, N. V. D. Giesen, J. S. Selker, and S. W. Tyler, "Calibrating single-ended fiber-optic Raman spectra distributed temperature sensing data," Sensors **11**(11), 10859–10879 (2011).
17. N. Van De Giesen, S. C. Steele-Dunne, J. Jansen, O. Hoes, M. B. Hausner, S. Tyler, and J. Selker, "Double-ended calibration of fiber-optic Raman spectra distributed temperature sensing data," Sensors **12**(5), 5471–5485 (2012).
18. I. Laarossi, M. A. Quintela-Incera, and J. M. López-Higuera, "Comparative experimental study of a high-temperature raman-based distributed optical fiber sensor with different special fibers," Sensors **19**(3), 574–587 (2019).
19. T. Reinsch and J. Henninges, "Temperature-dependent characterization of optical fibres for distributed temperature sensing in hot geothermal wells," Meas. Sci. Technol. **21**(9), 094022 (2010).
20. S. R. Baker, H. N. Rourke, V. Baker, and D. Goodchild, "Thermal decay of fiber Bragg gratings written in boron and germanium codoped silica fiber," J. Lightwave Technol. **15**(8), 1470–1477 (1997).
21. N. Liu, Y. Li, Y. Wang, H. Wang, W. Liang, and P. Lu, "Bending insensitive sensors for strain and temperature measurements with Bragg gratings in Bragg fibers," Opt. Express **19**(15), 13880–13891 (2011).
22. J. Li, Y. Du, and C. Liu, "FBG Strain Sensor Based on Thermal Stress Mechnism," in *Proc. 2008 Second. Int. Symp. on Intell. Inf. Technol. Appl.*, 640–642, (2008).
23. C. Campanella, A. Cuccovillo, C. Campanella, A. Yurt, and V. Passaro, "Fibre bragg grating based strain sensors: review of technology and applications," Sensors **18**(9), 3115–3142 (2018).
24. M. S. Ferreira, J. Vieira, C. Frias, and O Frazão, "Simultaneous measurement of strain and temperature using fiber Bragg grating sensors embedded in hybrid composite laminates," Meas. Sci. Technol. **22**(4), 045206 (2011).